Clays and Clay Minerals, Vol. 64, No. 2, 131–144, 2016.

HIGH-RESOLUTION TRANSMISSION ELECTRON MICROSCOPY (HRTEM) STUDY OF STACKING IRREGULARITY IN Fe-RICH CHLORITE FROM SELECTED HYDROTHERMAL ORE DEPOSITS

SAYAKO INOUÉ* AND TOSHIHIRO KOGURE

Department of Earth and Planetary Science, Graduate School of Science, The University of Tokyo, 7-3-1 Hongo, Bunkyo-ku, Tokyo 113-0033, Japan

Abstract—The structures of Fe-rich chlorite and berthierine and the formation mechanisms of 7 Å–14 Å interstratified minerals were not previously fully understood owing to the difficulties in analyzing them by X-ray diffraction (XRD). The present study characterizes Fe-rich chlorites in quartz veins of epithermal to xenothermal vein-type ore deposits without later structural modifications, based on high-resolution transmission electron microscopy (HRTEM) along with XRD examination and chemical analysis. Samples have a wide range of Fe/(Fe+Mg) ratios from 0.38 to 0.98 and tetrahedral Al substitution for Si from 0.94 to 1.44 atoms per formula unit (apfu). The variation in Fe content nearly parallels the tetrahedral Al content. The formation temperatures estimated by chlorite geothermometry range from 190ºC to 320ºC. In HRTEM, most of the samples showed interstratification between 7 Å, 14 Å, and/or (in some samples) smectite layers. Chlorites with relatively low Fe contents (Fe/(Fe+Mg) $\approx$ 0.4) were characterized by mostly 14 Å periodicity with the polytype II*bb*. In contrast, interstratification of 7 Å and 14 Å layers predominated with increasing Fe content and the proportion of 7 Å layers exceeds 80% in Fe-rich samples with Fe/(Fe+Mg) > 0.9. The 7 Å component layer approximated Fe-rich berthierine based on the chemical composition. Layer stacking structures in the Fe-rich samples were complex, and characterized by disorder of 7 Å and 14 Å layers, differences in the polarity of the tetrahedral sheets, variations of the slant of the octahedral sheets, and positional disorder between octahedral and tetrahedral sheets involving the hydrogen bonding, as indicated from HRTEM observations along the Y_i directions of the phyllosilicates. The complex stacking structures observed in Fe-rich samples suggest that irregularity was controlled by neither the Fe/(Fe+Mg) ratio nor the formation temperature; stacking was controlled by kinetic factors in the process of mineral precipitation under disequilibrium conditions.

Key Words—Berthierine, Chlorite, HRTEM, Polytypism, Serpentine-Chlorite Interstratified Mineral.

INTRODUCTION

Trioctahedral chlorite has a 14 Å unit structure consisting of alternation of the 2:1 layer and an interlayer hydroxyl sheet. Its general chemical formula is $(R^{2+}_a R^{3+}_b \square_c)_6(Si_{4-x}R^{3+}_x)_4O_{10}(OH)_8$, where R^{2+} represents divalent cations, mainly Mg and Fe(II); R^{3+} are trivalent cations such as Al and Fe(III); and $\square$ is the vacancy among the octahedral sites; charge balance requires that $b-x = 2c$ (*e.g.* Brindley, 1982; Bailey, 1988a). The formula of berthierine, a serpentine mineral with a 7 Å unit structure consisting of 1:1 layers, is equal to half of the chlorite formula. Structurally, chlorite and berthierine (or serpentine) are characterized by a variety of polytypic groups (*e.g.* Bailey, 1988a, 1988b). Moreover, interstratification of the two types of minerals commonly occurs in natural samples. Changes in the polytypic structure, interstratification, and variations in the chemical composition are understood to be a function of temperature and possibly many other intensive variables such as total pressure, partial pressures of oxygen and sulfur, and activities of metal cations in solution (*e.g.* Bailey, 1988a) and certainly rate of cooling (kinetics).

Trioctahedral chlorites are common minerals in sedimentary, low- to medium-grade metamorphic, and hydrothermally altered rocks. Berthierine is reported mainly from sedimentary rocks that have undergone early diagenesis (*e.g.* Velde, 1985; Meunier, 2005). In addition, occurrences of Fe-rich chlorite and berthierine were reported from oolitic iron stones, iron formations, and volcanogenic massive sulfide deposits (*e.g.* Velde, 1985; Slack and Coad, 1989). According to field and laboratory studies (see reviews by Velde, 1985 and Bailey, 1988a and references therein), berthierine may be a metastable phase and probably transforms to chlorite with increasing temperature. The transformation occurs at 70–200ºC by way of interlayering of the two minerals (*e.g.* Velde, 1985; Hillier, 1993; Hornibrook and Longstaffe, 1996; Billault *et al*., 2003; Meunier, 2005). Previous studies used powder XRD methods and microprobe analysis; consequently the details of the transformation mechanism are not understood well. High-resolution transmission electron microscopy is a complementary tool to examine the transformation mechanism of fine-grained minerals at the atomic

* E-mail address of corresponding author:
inouesayako@gmail.com
DOI: 10.1346/CCMN.2016.0640205

scale. The HRTEM observations by Xu and Veblen (1996) indicated that berthierine transformed to chlorite such that the product phase inherited the basic polytypic structure of the reactant phase by way of an antiphase boundary between the two layers. Banfield and Bailey (1996) showed a similar transformation from serpentine to clinochlore in metamorphosed serpentinite. These researchers proposed a different mechanism by considering the stability of the polytypic structure of product chlorite. In contrast, Slack *et al*. (1992) and Jiang *et al*. (1992) examined the structural relationship between berthierine and chlorite in a volcanogenic massive sulfide ore deposit of Archean age that was metamorphosed at 300–400ºC. These researchers inferred that chlorite was replaced by berthierine through the topotactic transformation from chlorite to berthierine, based on lattice fringe images.

In addition to the studies of transformation between berthierine and Fe-rich chlorite, the precipitation of extremely Fe-rich chlorite in association with quartz and sulfide deposition was studied in specific epithermal to xenothermal (in the sense of Buddington, 1935) vein-type ore deposits (*e.g*. Nakamura, 1970; Shirozu, 1978; Inoue *et al*., 2010). Details of chemical and structural properties of these chlorites are, however, not well understood. The purpose of this study was to characterize chlorites from several hydrothermal ore deposits in Japan. This study considered chemical and structural aspects by HRTEM examination, together with powder XRD and chemical analysis and focused on understanding the stacking structure of Fe-rich chlorite minerals, and comparing them to those of more common intermediate Mg, Fe-chlorites from epithermal vein-type ore deposits. Special emphasis was placed on the notation of disorder in the stacking structure of chlorite-serpentine in Fe-rich chlorite and on the characterization of the component layers.

SAMPLES

Seven chlorite samples were studied from epithermal to xenothermal vein-type ore deposits in Japan: one each from Toyoha, Arakawa, and Ashio, two from Osarizawa, and two from drill cores in the geothermal field adjacent to the Toyoha deposit. All deposits formed in the Miocene to Pliocene, and no evidence of metamorphism or deformation after formation is present (Shikazono, 2003). Chlorites studied here showed the characteristics of precipitates under optical and scanning electron microscopes (*e.g*. Inoue *et al*., 2012).

The Toyoha deposit, Hokkaido Prefecture, consists of a network of veins with polymetallic mineralization of Pb, Zn, Ag, Mn, In, Cu, Bi, Sn, *etc*. Hydrothermal activity with mineralization started at ~3 Ma and remains active. Chlorites from the mineralized vein, the Soya vein, in the Toyoha deposit, and drill cores (referred to as TH-2 by Inoue *et al*., 2010, 2012) from the adjacent geothermal field were investigated here. Soya chlorite is a gangue mineral from a quartz vein, associated with sphalerite and pyrite. Homogenization temperatures of fluid inclusions in quartz ranged from 210 to 261ºC, on average 233ºC (A. Inoue, pers. comm., 2012; shown in Table 1). Chlorites from drill core TH-2, which were collected at depths of 680 m and 894 m from fill veinlets in hydrothermally altered andesite, associated with quartz and pyrite. The hydrothermal alteration and homogenization temperatures of fluid inclusions in core TH-2 were described by Inoue *et al.* (2010, 2012).

The Osarizawa and Arakawa deposits, Akita Prefecture, are typical Cu-Pb-Zn epithermal vein-type ore deposits. Chlorite was collected from two mineralized quartz veins, the Ishikirizawa and Unotori veins in the Osarizawa deposit, and from the contact between a barren quartz vein and shale country rock in Arakawa. Chlorites from Osarizawa are associated with chalcopyrite, sphalerite, galena, and pyrite; those from Arakawa with pyrite and hematite. Homogenization temperatures of fluid inclusions in quartz ranged from 248 to 356ºC, on average 279ºC, for Ishikirizawa; from 225 to 320ºC, on average 269ºC, for Unotori; and from 188 to 287ºC, on average 247ºC, for Arakawa (Table 1).

The Ashio deposit, Tochigi Prefecture, is classified as a xenothermal, polymetallic vein-type ore deposit (Imai *et al.*, 1975). Despite the limited number of microthermometric studies in Ashio, the ore formation occurred at temperatures of > 300ºC (Shikazono, 2003).

METHODS

The samples were crushed gently and sonicated in distilled water. The clay-size fraction was separated by repeated decantation. Because the samples from Soya, Ishikirizawa, and Unotori contained significant amounts of impurities such as sulfide minerals, the clay fractions were further separated by Na-polytungstate densimetry (Gregory and Johnston, 1987; Cassagnabère, 1998). The separated clay suspension was sedimented onto glass slides and air-dried to prepare oriented mounts. Random powder mounts were prepared by the side-loading method (Moore and Reynolds, 1989).

Powder XRD patterns were acquired using a RINT-Ultima+ diffractometer (Rigaku, Tokyo, Japan) with a Cu X-ray tube, Ni filter, and silicon strip X-ray detector (Rigaku D/teX Ultra). CuKα radiation was produced at 40 kV and 30 mA. A measurement condition of 0.25º divergence slit, 10 mm mask confining the beam width, and 8 mm anti-scatter slit was used. The pattern was obtained every 0.02º2θ at a scan rate of 0.5º2θ/min over the range of 2 to 75º2θ.

Chemical analyses of the chlorites were performed on petrographic thin sections using a Kevex Sigma energy-dispersive X-ray spectrometer (EDS: Kevex, Foster City, California, USA) attached to a Hitachi S-4500 scanning

https://doi.org/10.1346/CCMN.2016.0640205 Published online by Cambridge University Press

Table 1. Chemical composition of samples. Structural formulae were calculated on the basis of O = 14. N = number of analyses.

			Toyoha								Osarizawa			
	Ashio N = 19	STD[d]	Soya N = 28	STD	TH-2-680 N = 10	STD	TH-2-894 N = 10	STD	Arakawa N = 17	STD	Unotori N = 23	STD	Ishikirizawa N = 21	STD
SiO_2	21.62	0.36	22.51	1.35	24.85	1.14	26.12	1.49	31.02	1.75	28.95	0.93	28.59	0.50
Al_2O_3	22.46	0.53	20.02	0.86	16.65	2.29	18.01	0.66	23.77	1.79	17.38	0.64	16.22	0.63
FeO[a]	41.69	0.29	36.60	5.16	37.40	4.24	25.68	2.36	35.70	4.83	22.19	2.97	20.48	1.86
MnO	0.06	0.05	2.26	2.13	1.12	2.75	8.08	3.24	0.00	0.00	0.84	0.10	0.81	0.14
MgO	0.37	0.06	2.40	2.56	3.89	0.30	8.08	4.11	9.51	2.52	16.53	1.74	18.42	1.17
Total	86.21	0.93	83.79	4.24	83.90	1.89	85.98	1.02	100.00		85.88	2.97	84.53	1.26
Structure formula on the basis of O=14														
Si	2.56	0.02	2.70	0.04	2.97	0.12	2.94	0.07	2.93	0.10	3.06	0.05	3.05	0.02
^{IV}Al	1.44	0.02	1.30	0.04	1.03	0.12	1.06	0.07	1.07	0.10	0.94	0.05	0.95	0.02
ΣTetrahedral cations	4.00		4.00		4.00		4.00		4.00		4.00		4.00	
^{VI}Al	1.69	0.03	1.54	0.08	1.31	0.13	1.33	0.04	1.58	0.15	1.22	0.06	1.09	0.04
Fe^{2+}	4.12	0.05	3.69	0.57	3.76	0.56	2.43	0.30	2.84	0.47	1.96	0.25	1.83	0.18
Mn	0.01	0.01	0.22	0.20	0.11	0.03	0.78	0.33	0.00	0.00	0.07	0.01	0.07	0.01
Mg	0.07	0.01	0.42	0.43	0.68	0.46	1.33	0.63	1.33	0.32	2.60	0.25	2.93	0.15
ΣOctahedral cations	5.89		5.87		5.86		5.87		5.75		5.85		5.92	
No. of vacancies	0.11		0.13		0.14		0.13		0.25		0.15		0.08	
Fe/(Fe+Mg)	0.98		0.90		0.85		0.65		0.68		0.43		0.38	
Formation T (°C)[b]	321	33	281	46	214	72	222	23	187	25	200	30	270	33
T_h (°C)[c]	~300[e]		233	22	204	15	269	5	247	32	269	27	279	38

a: Total iron as FeO.
b: Formation temperature estimated using the chlorite geothermometer developed by Bourdelle *et al*. (2013).
c: Homogenization temperatures of fluid inclusions in quartz (unpublished data by A. Inoue).
d: Standard deviation
e: cited from Shikazono (2003)

electron microscope (SEM: Hitachi, Tokyo, Japan) with a cold field-emission gun operated at 15 kV.

Specimens for examination by TEM were prepared using a focused ion beam (FIB) instrument with micro-sampling system (Hitachi FB-2100, Hitachi, Tokyo, Japan). Petrographic thin sections were cut into 5 mm squares to be accommodated in the FIB chamber, and coated with carbon to prevent charge accumulation during the FIB process. In the FIB procedure, tungsten was deposited on the surface of the target area. Then trenches of ~5 μm in depth were formed around the target area with a high energy (30 keV) Ga ion beam, and a fragment of each thin section was transferred onto a crescent-shape copper grid using a micro-sampling system. The fragment was thinned to <100 nm with a low-energy Ga ion beam of 10 keV to minimize surface amorphization caused by the bombardment of Ga ions.

Specimens prepared by FIB were examined using a TEM (JEM-2010UHR, JEOL, Tokyo, Japan) operated at 200 kV with a nominal point resolution of ~ 0.2 nm. HRTEM images were recorded using a Gatan MSC 794 bottom-mounted CCD camera, then processed using the Wiener-filter (Marks, 1996; Kilaas, 1998) developed by K. Ishizuka (HREM Research Inc., Saitama, Japan) which was implemented in a Gatan Digital Micrograph to remove noise contrast. Because the contrast in an HRTEM image depends on the sample thickness and defocus condition, the HRTEM images were recorded at sufficiently thin areas of the TEM specimens and with a proper defocus condition to make suitable correspondence between the images and crystal structures, following Kogure and Banfield (1998) and Kogure *et al.* (2001). The HRTEM images were recorded along one of the Y_i directions (i= 1 to 3) defined by Bailey (1969), and the polytypic groups of serpentine and chlorite layers were identified based on the image simulations made by Kogure and Banfield (1998) and Kogure *et al.* (2001).

RESULTS

Chemical composition

Structure formulae were calculated based on 14 oxygen atoms; iron cations were regarded as divalent (Table 1). Although the standard deviations for some element abundances in some of the samples were large, no zonation of elements was observed within a single grain of chlorite under SEM. The Fe/(Fe+Mg) ratios range from 0.38 to 0.98. TH-2-894 contains significant Mn compared to the other samples. Tetrahedral Al (^{IV}Al) content is in the range of 0.94−1.44 atoms per formula unit (apfu). The ^{IV}Al content parallels the Fe/(Fe+Mg) ratios in octahedral sites. In particular, the Ashio sample is characterized by large amounts of ^{VI}Fe(II) (4.12 apfu) and ^{IV}Al (1.44 apfu) (Figure 1). This correlation between the ^{IV}Al and Fe/(Fe+Mg) is typical of the chemical composition of chlorite (*e.g.* Bailey and Brown, 1962; Foster, 1962; Bailey, 1988a). The composition is comparable to berthierine from the Kidd Creek volcanogenic massive sulfide ore deposit (Slack and Coad, 1989; Slack *et al.*, 1992; Jiang *et al.*, 1992) and data from sedimentary rocks (*e.g.* Brindley, 1982; Iijima and Matsumoto, 1982), because a 7 Å diffraction peak was dominant in the XRD pattern of the Ashio sample (see Figure 2). The negative layer charges generated by Al substitutions for Si may be compensated by Al substitutions and small numbers of vacancies in the octahedral sheets (Brindley, 1982).

Bourdelle *et al.* (2013) proposed a geothermometer to estimate the temperature of chlorite formation using chemical composition without considering the effect of ferrous and ferric iron concentrations. Inoue *et al.* (2009) noted that their geothermometer is applicable to berthierine. On this basis, the chlorite geothermometer by Bourdelle *et al.* (2013) was applied to the present samples even with their interlayering of 7 Å layers. The estimated temperatures of formation ranged from ~190ºC to 320ºC, generally near the respective homogenization temperatures of fluid inclusions in associated quartz (Table 1). Despite large standard deviations in the formation temperatures and the homogenization temperatures, all samples studied here formed at >190ºC; these formation temperatures are higher than those for sedimentary berthierine (*e.g.* Velde, 1985; Meunier, 2005).

XRD

XRD patterns of oriented samples suggested that all samples contain impurities such as illite, quartz, pyrite, and/or chalcopyrite (examples are shown in Figure 2). The 14 Å diffraction peak of chlorite was present in all samples, but the intensity ratios of the 001/002 diffraction peaks varied. The intensity ratio of the 001/002

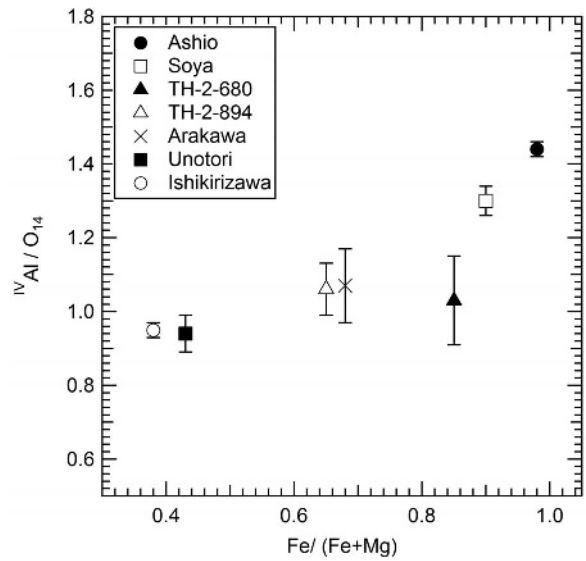

Figure 1. Relationship between ^{IV}Al and Fe/(Fe+Mg) in the samples. Error bars indicate the standard deviations.

https://doi.org/10.1346/CCMN.2016.0640205 Published online by Cambridge University Press

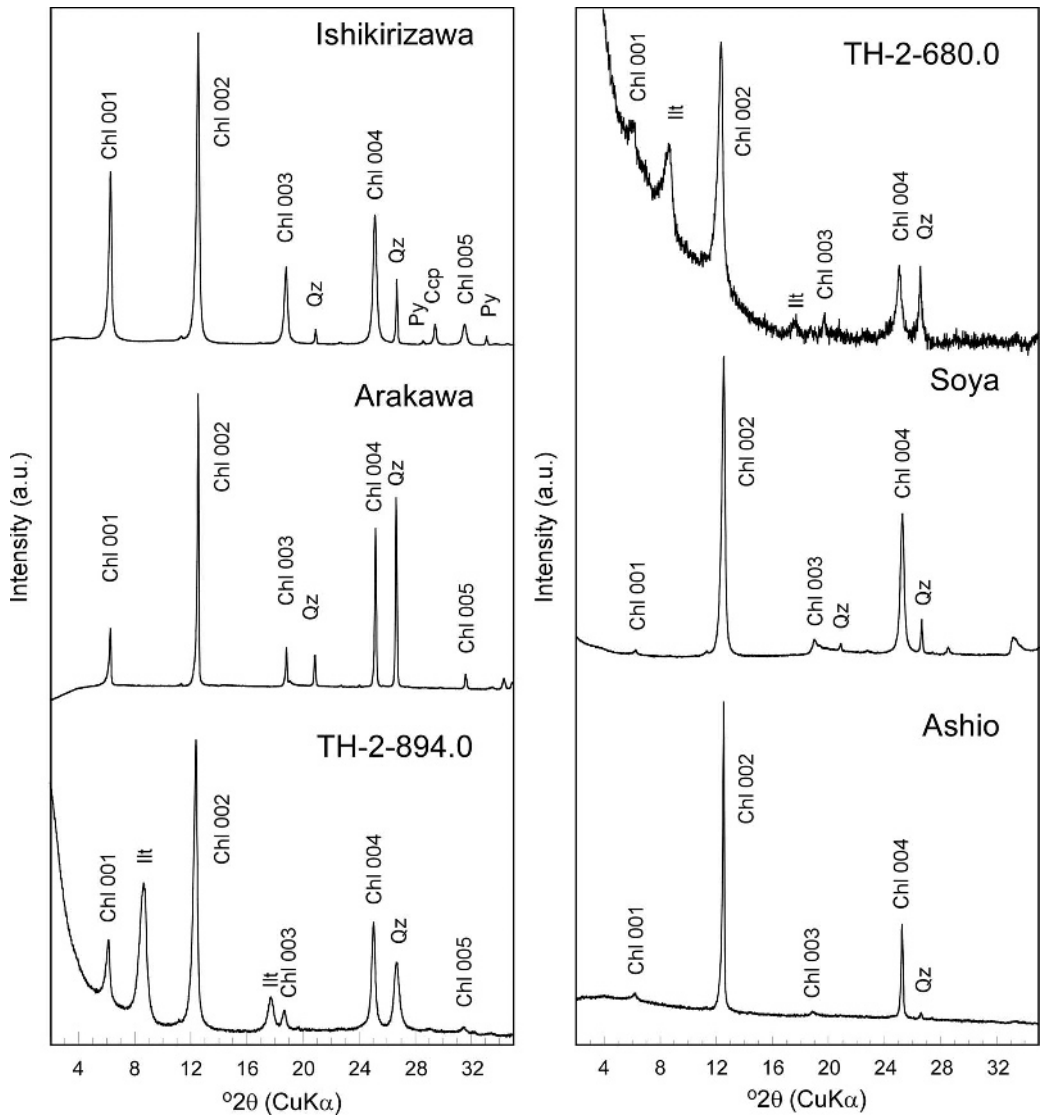

Figure 2. Examples of one-dimensional powder XRD patterns of oriented chlorite samples. Chl: chlorite, Ilt: illite, Qz: quartz, Py: pyrite, Ccp: chalcopyrite; a.u.: arbitrary units.

peaks of the Unotori sample was similar to that of the Ishikirizawa sample (XRD pattern of the Unotori sample not shown here). Ethylene glycol treatment showed no expandable component; diffraction peaks from long spacings diagnostic of regular interstratification were not observed in any sample.

For 7 Å and 14 Å interstratifications, Reynolds *et al.* (1992) indicated that interlayering of berthierine and chlorite is suggested by peak-broadening of odd-order 00*l* diffraction peaks. Such broadening in odd-order 00*l* diffraction peaks was not apparent in the samples studied here (Figure 2). Reynolds (1988) and Reynolds *et al.* (1992) noted that if the amounts of berthierine component layers are >20% in interstratified chlorite, a berthierine component cannot be detected by XRD because these diffraction peaks would be too weak and broad. Moreover, samples containing appreciable Fe also produce weak 00*l*, $l = 2n+1$ diffraction peaks. Thus, samples from Unotori, Ishikirizawa, Arakawa, and TH-2-894 appeared to be chlorite dominated, whereas samples from TH-2-680, Soya, and Ashio consisted of berthierine ± chlorite ± berthierine-chlorite interstratification.

The XRD patterns of randomly oriented Unotori, Soya, and Ashio samples in the range of 30º−75º2θ were compared with calculated powder XRD intensities with $k = 3n$ reflections (orthohexagonal cell setting) for I*bb* and II*bb* of Mg-chlorite and groups C and A of serpentine (Figure 3), using the structure parameters of Bailey and Brown (1962) and Bailey (1969). The XRD pattern of the Unotori sample was consistent with the structure of chlorite-II*bb* (Figure 3) after introducing peak shifts from composition-dependent cell dimensions (see Table 1) in

https://doi.org/10.1346/CCMN.2016.0640205 Published online by Cambridge University Press

the calculated pattern. Polytypic groups of Ishikirizawa, Arakawa, and TH-2-894 chlorites were also assigned to II*bb* (data not shown), although the considerable interference from illite was apparent in the XRD patterns. The profiles of Soya, Ashio, and TH-2-680 samples could not be assigned to one type of polytypic group of serpentine or chlorite, although some of the diffraction peaks in the diffraction profiles were diagnostic of I*bb* of chlorite and group A and C of serpentine (Figure 3).

TEM

Low-magnification HRTEM images of select samples showed that most samples were characterized by continuous, parallel stacks of layers without inclined contact with contiguous packets, and a few dislocations (Figure 4). In samples with low Fe contents (Fe/(Fe+Mg) $\approx$ 0.4), *i.e.* Ishikirizawa and Unotori, 14 Å layers dominate and 7 Å layers were seldom observed

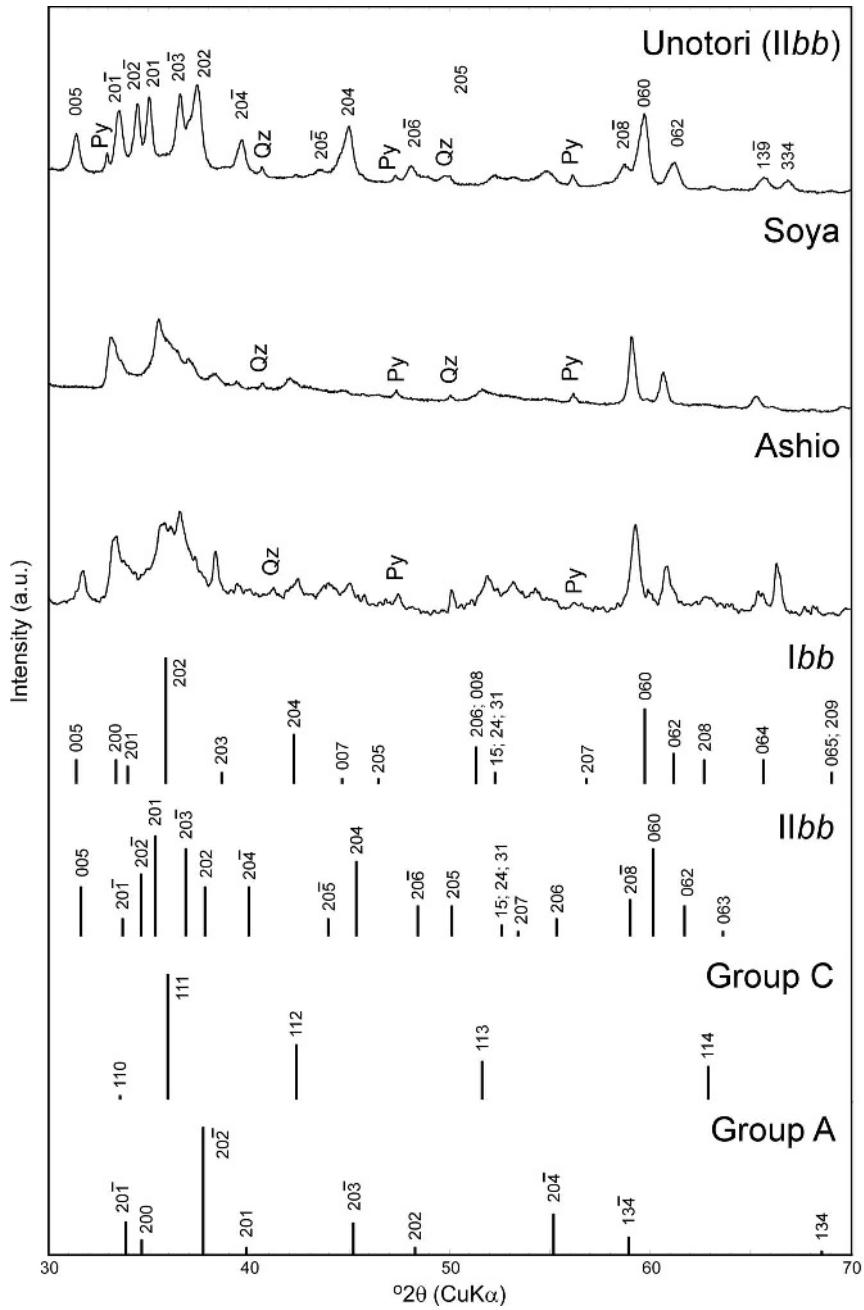

Figure 3. Examples of powder XRD patterns from randomly-oriented samples to identify polytypic groups and the positions of peaks which are characteristics of representative polytypic groups of chlorite (I*bb* and II*bb*) and serpentine (groups C and A). Polytypic groups in parentheses are possible candidates for each sample. Qz: quartz, Py: pyrite; a.u.: arbitrary units.

https://doi.org/10.1346/CCMN.2016.0640205 Published online by Cambridge University Press

(Figures 4a and b). Layers with 24 Å periodicity were observed in some chlorite packets from Unotori (Figure 4b), which is probably a result of regular interstratification of chlorite-smectite (*e.g.* Beaufort *et al.*, 1997; Kogure *et al.*, 2013), because smectite layers collapsed to ~10 Å under vacuum conditions, and no K was detected by chemical analysis by TEM-EDS. The proportion of 24 Å layers is low, and hence not detected by XRD. The interlayering of 7 Å layers was frequently encountered in samples with high Fe contents (Fe/(Fe+Mg) > 0.8), such as the Ashio sample (Figure 4d). Comparing the Fe/(Fe+Mg) ratios of samples (Table 1), the proportions (%) of 7 Å layers determined from several HRTEM images for each sample were nearly proportional to the Fe content: 0% (Ishikirizawa), 0% (Unotori), 8% (Arakawa), 14% (TH-2-894), 73% (Soya), 79% (Ashio), and 88% (TH-2-680), and independent of the formation temperature. No domain-like distribution of 7 Å and 14 Å layers was observed by low magnification TEM.

Selected area electron diffraction (SAED) patterns of Ishikirizawa, Arakawa, and TH-2-680 along one of the Y_i directions showed that the intensity of odd 00*l* spots for chlorite decreased with increasing proportion of 7 Å layers (Figures 5a, b, and c, respectively). The reciprocal lattices are oblique for Ishikirizawa and Arakawa (Figure 5a,b). Polytypic groups of Ishikirizawa and Arakawa were assigned to chlorite-II*bb*; that of Unotori

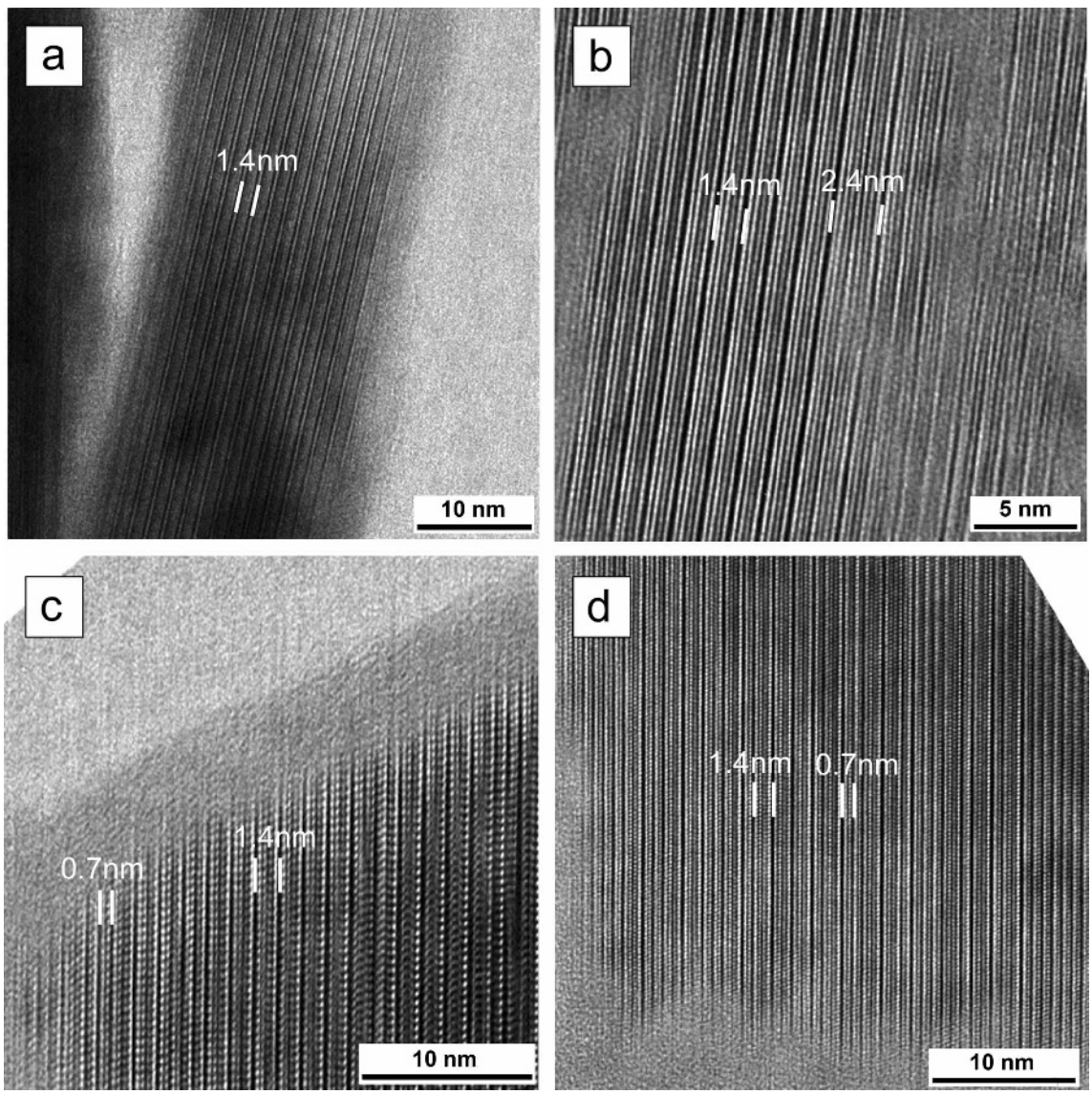

Figure 4. HRTEM images with a relatively low magnification, showing the layer stacking in the samples of (a) Ishikirizawa, (b) Unotori, (c) Arakawa, and (d) Ashio. Images in parts a, b, and d were recorded along one of the Y_i directions and that in part c along one of the X_i directions.

https://doi.org/10.1346/CCMN.2016.0640205 Published online by Cambridge University Press

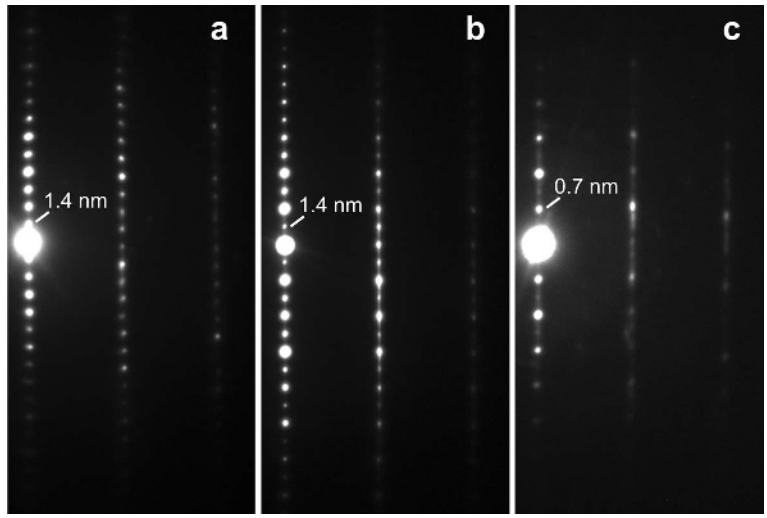

Figure 5. SAED patterns of several samples with varying proportions of 7 Å layers taken along one of the Y_i directions. (a) Ishikirizawa, (b) Arakawa, and (c) TH-2-680.

was also assigned mainly to II*bb*, but I*ba* stacking was locally observed in HRTEM images of the sample (Figure 6). Determination of the polytypic group of TH-2-680 (equivalent to Ashio and Soya, though not shown here) from the SAED pattern was not possible because of intensive streaking along the c^* direction (Figure 5c). Hence, direct observations by HRTEM were important to understand the structure of these extremely Fe-rich samples.

The stacking structures in Ashio and Soya samples are disordered and are difficult to describe using conventional polytype notation such as I*bb* and II*bb* for chlorite layers, or groups A and C for serpentine layers. This difficulty was a result of interstratification at a fine scale and the 7 Å layers occurring with opposite polarities (Figure 7). The lateral contacts of the opposite polar 7 Å layers were observed on the HRTEM images (Figure 7 and white boxes). To demonstrate the

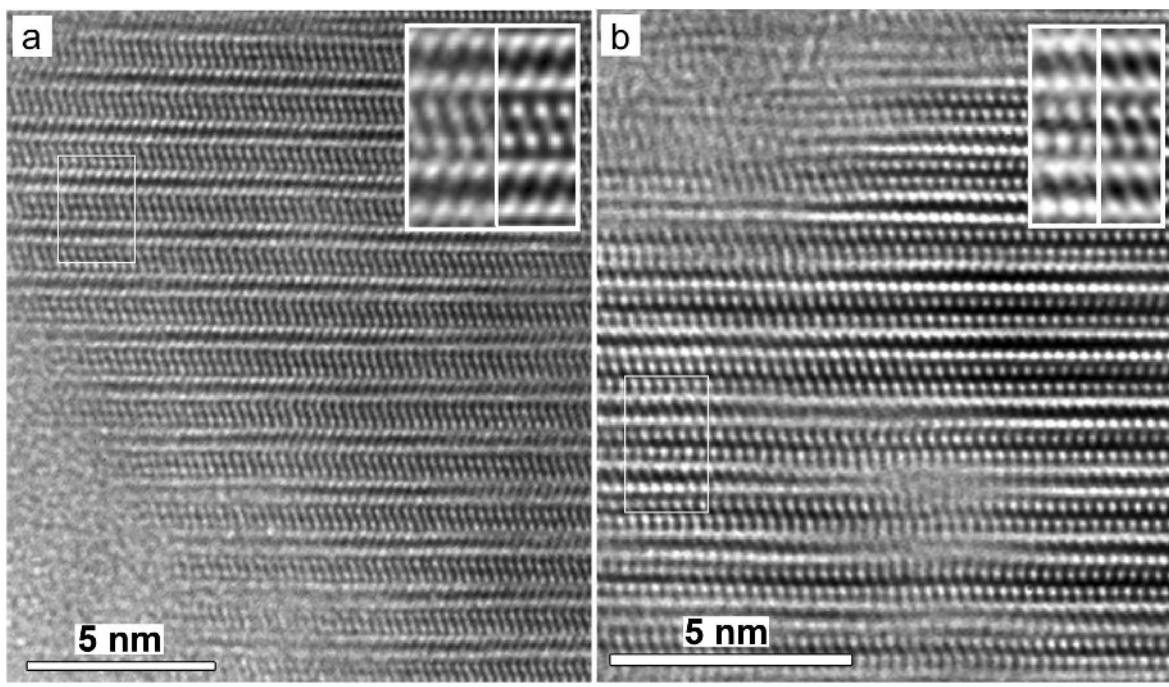

Figure 6. HRTEM images recorded along one of the Y_i directions of (a) chlorite-II*bb* from Ishikirizawa and (b) chlorite-I*ba* from Unotori. The inset images are the magnified images of the area indicated by white boxes (left) with the simulated images (right) showing the unit structure. HRTEM image simulation was carried out following Kogure and Banfield (1998). Simulation parameters are: defocus = −40 nm (Scherzer focus); specimen thickness = 2 nm.

https://doi.org/10.1346/CCMN.2016.0640205 Published online by Cambridge University Press

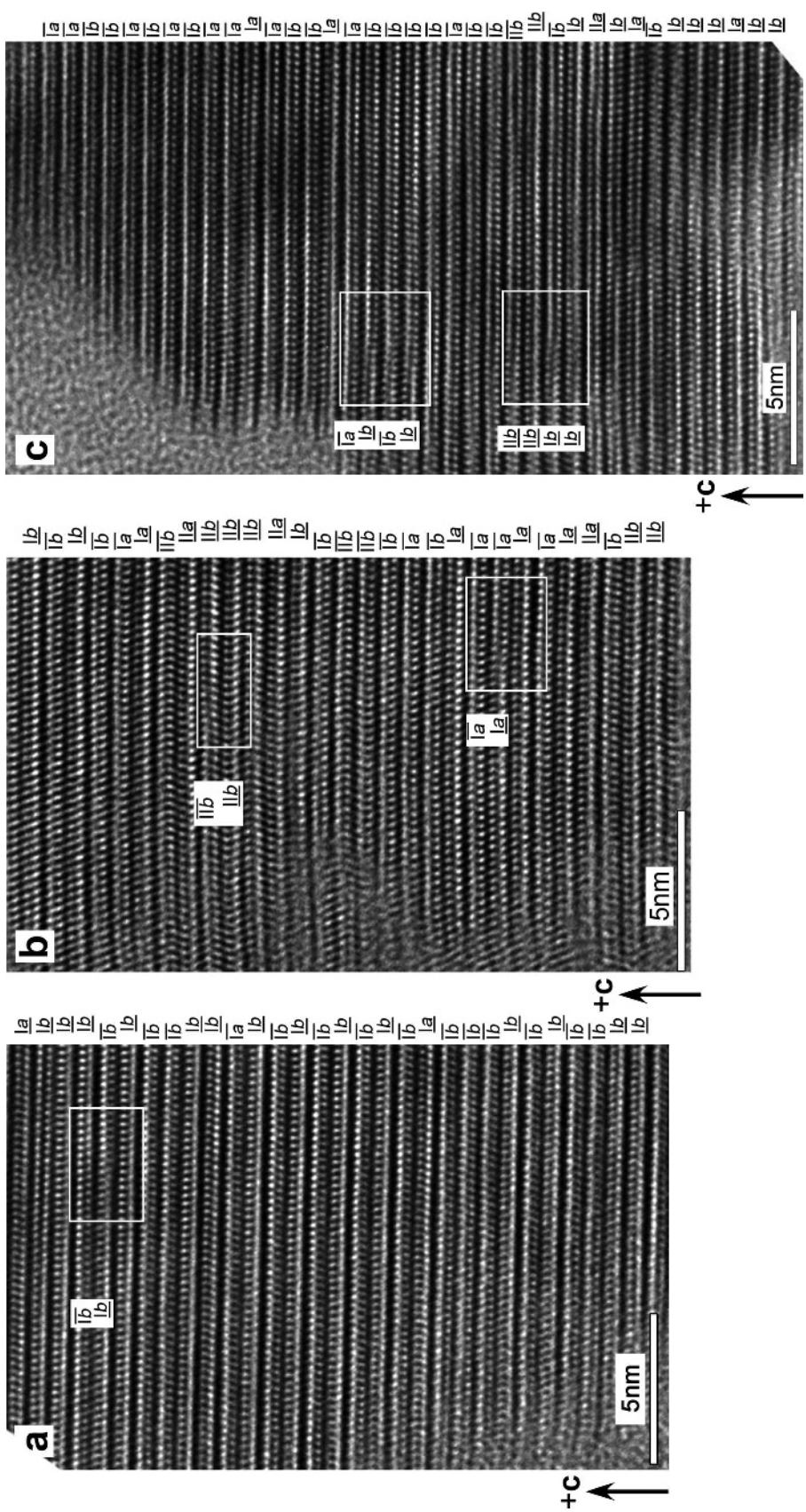

Figure 7. HRTEM images recorded along one of the Y, directions of 7 Å and 14 Å interstratified minerals from (a) Ashio, (b) Soya, and (c) TH-2-680. The symbol for the new notation method to describe the stacking structure of each layer is denoted at the right-hand side of the images (see text for detail), and white boxes on the images indicate the lateral contacts of modules of opposite polarity.

https://doi.org/10.1346/CCMN.2016.0640205 Published online by Cambridge University Press

irregularity of such stacking structure completely, a new notation is proposed and the details of the stacking structure are further discussed below. In this study, the interlayering of the 7 Å layers with opposite polarities, a mixture of different polytypic groups, and the lateral contacts of opposite polar 7 Å layers are collectively referred to as the irregularity of the structure.

DISCUSSION

Layer stacking in interstratification

For the integrated description of the stacking for the interlayering of 7 Å and 14 Å layers at a fine scale, a new notation was employed, as follows. All component layers are described as 7 Å thick. Thus, the chlorite layer is divided into two layers when the structure is viewed along one of the Y_i directions: one layer is between the cation plane of the upper interlayer octahedral sheet and that in 2:1 layer, and another between the octahedral cation plane of the 2:1 layer and that of lower interlayer octahedral sheet (Figure 8). If the component layer contains the tetrahedral sheet with −c axis-oriented apical oxygens, the component layer is termed the −c module and expressed with over-bar (¯), and that with the +c axis-oriented apical oxygens is termed the +c module with under-bar (_) (Figure 8). The octahedral slant of each module is defined following that of Bailey and Brown (1962). Hence, if the slant directions of the octahedral sheets at the lower and upper boundaries of the component layer are in the same direction, the layer is defined as type I, and if the slant directions of the octahedral sheets are anti-parallel, the layer is defined as type II (Figure 8). If the tetrahedral cations are located just above or below the octahedral cations across the hydrogen bond, then the relationship between them is termed type *a* stacking; and if the tetrahedral cations are laterally shifted relative to the octahedral cations, then the structure is type *b* stacking (Figure 8). Using this notation, chlorite-I*bb* and -c and +c serpentine of group C are expressed as $\overline{\text{I}b}\underline{\text{I}b}$, $\overline{\text{I}b}\overline{\text{I}b}$, and $\underline{\text{I}b}\underline{\text{I}b}$, respectively. The

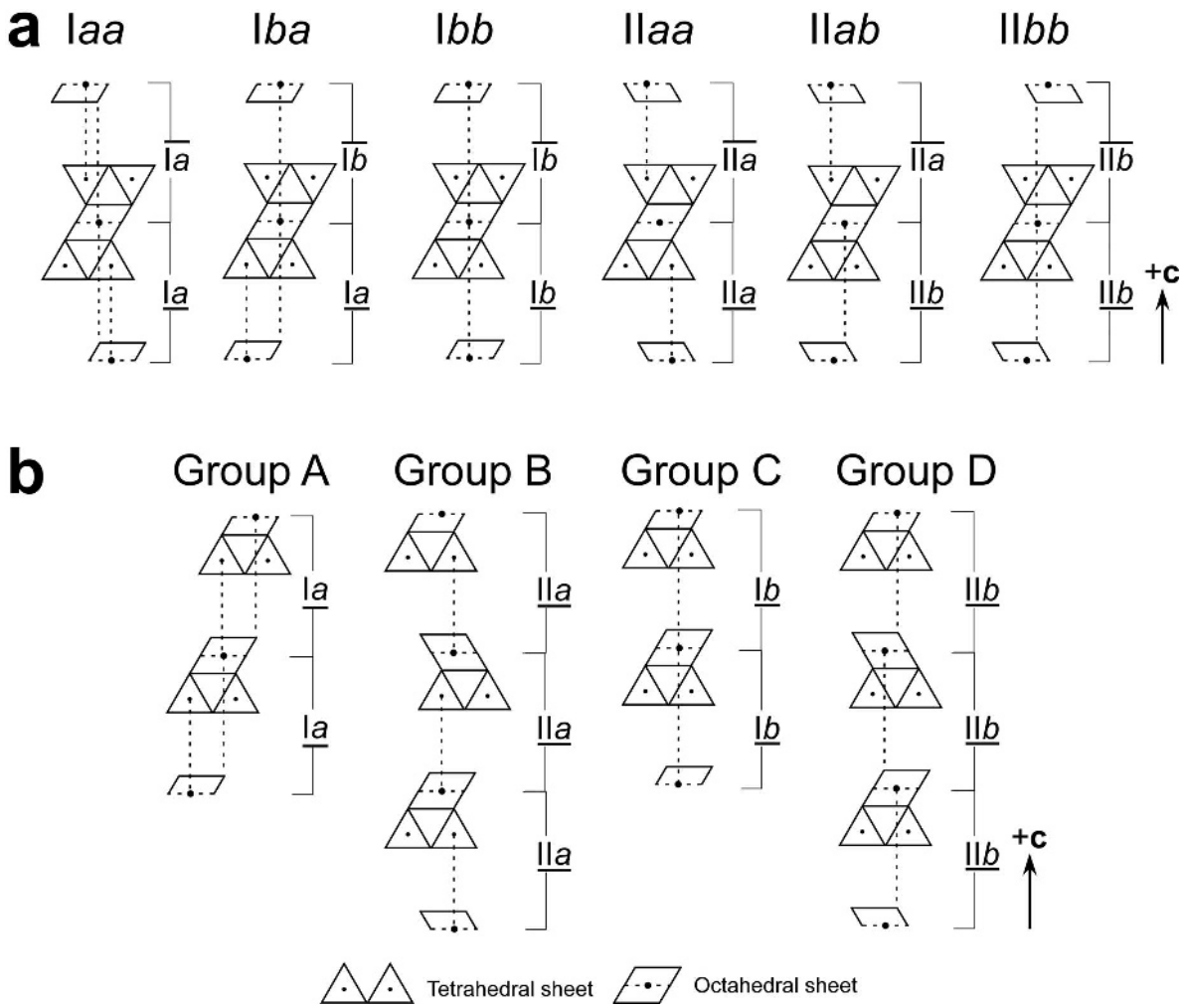

Figure 8. Schematic diagrams showing the correspondence between polytypic notations proposed in the present study and that of Shirozu and Bailey (1965) for (a) chlorite and of Bailey (1969) for (b) serpentine.

https://doi.org/10.1346/CCMN.2016.0640205 Published online by Cambridge University Press

conventional polytypic notations for chlorite and serpentine can be described using the new notations (Figure 8). Note that this notation is applicable to the stacking configurations that can only be observed in HRTEM, and is not applicable to the XRD data directly.

The stacking structures of interstratified minerals from Ashio, Soya, and TH-2-680 were described using the new notation, as given in the right-hand side of the HRTEM images (Figure 7). In the Ashio sample (Figure 7a), both the −c and +c 7 Å layers were found within a small packet in approximately equal proportions, but the two modules did not alternate as expected for pure chlorite. The two modules linked preferentially with the type I*b* stacking, although the stacking was perturbed locally by type I*a* (Figure 7a). In the Soya sample, the proportions of −c and +c layers resembled that in Ashio (Figure 7b). In contrast, the proportion in TH-2-680 was very different and the amount of downward layers was almost twice that of upward layers (Figure 7c). Furthermore, different types of shift (*a* and *b*) and octahedral slant (I and II) mixed irregularly in Soya and TH-2-680. The 14 Å layer of $\overline{\mathrm{II}}b\underline{\mathrm{I}b}$, stacking which cannot be categorized into any of the six polytypic groups, was observed in Soya (Figure 7b). The irregularity was more obvious in Soya than in TH-2-680. The degree of irregularity in layer stacking may be controlled by many factors, *e.g.* chemical composition, formation temperature, transformation mechanism, and kinetics of mineral precipitation such as crystal growth rate. The data (Table 1) indicated that the Fe/(Fe+Mg) ratio and the ^{IV}Al content decrease in the order of Ashio, Soya, and TH-2-680 and the formation temperatures of these samples are in the range 190−300ºC. The order of the Fe/(Fe+Mg) ratio and the ^{IV}Al content was inconsistent with the order of increasing irregularity; hence, the three factors can be excluded from the principal causes of the irregularity. Kinetic factors during crystal growth are suspected to be the main causes of formation of the complex irregularities in the stacking of 7 Å and 14 Å layers.

Lateral relation between 7 Å and 14 Å layers

Considering the transformation mechanism between 7 Å and 14 Å layers, Baronnet (1992) noted that if the serpentine-chlorite interstratified mineral is an intermediate stage of topotactic transformation from serpentine to chlorite (or *vice versa*), the polytypic group of the reactant phase must be inherited by the product phase. Many studies have used the β angle as measured on SAED patterns to identify the transformation mechanism (*e.g.* Jiang *et al*., 1992; Banfield and Bailey, 1996; Xu and Veblen, 1996). For the case where the β angle of serpentine was 90º in the transformation from serpentine to chlorite, for instance, Xu and Veblen (1996) simply assumed that serpentine-2*H* (group D) transformed to chlorite-II*ab*, thereby maintaining β = 90º. Using the present notation method, the transformation is described from $\overline{\mathrm{II}}b\overline{\mathrm{II}}b\overline{\mathrm{II}}b$ to $\overline{\mathrm{II}}a\underline{\mathrm{II}}b$. Note that II*ab* is not a stable polytypic group of chlorite. Banfield and Bailey (1996), therefore, constructed another structure model to explain the conversion from serpentine of group D to chlorite-I*bb* ($\overline{\mathrm{II}}b\overline{\mathrm{II}}b\overline{\mathrm{II}}b$ to $\overline{\mathrm{I}b}\underline{\mathrm{I}b}$ by the present notation) by changing the direction of octahedral slant at the lateral contact between 7 Å and 14 Å layers. In the present study, the lateral contact was encountered infrequently in the interstratified structure as described above (for example, white boxes in Figure 7). The lateral contacts are expressed as $\overline{\mathrm{I}b}\underline{\mathrm{I}b}\mathrm{I}b$ and $\overline{\mathrm{I}b}\overline{\mathrm{I}b}\underline{\mathrm{I}b}$ in Ashio, $\overline{\mathrm{II}}b\underline{\mathrm{II}}b$ and $\underline{\mathrm{II}b\mathrm{II}b}$, and $\overline{\mathrm{I}a}\underline{\mathrm{I}a}$ and $\underline{\mathrm{I}a\mathrm{I}a}$ in Soya, and $\overline{\mathrm{I}a}\underline{\mathrm{I}b}\overline{\mathrm{I}b}\underline{\mathrm{I}b}$ and $\overline{\mathrm{I}a\mathrm{I}b}\mathrm{I}b$, and $\underline{\mathrm{II}b\mathrm{II}b\mathrm{I}b\mathrm{I}b}$ and $\overline{\mathrm{II}}b\underline{\mathrm{II}}b\overline{\mathrm{I}b}\underline{\mathrm{I}b}$ in TH-2-680. Close examination of HRTEM images revealed that the model of Xu and Veblen (1996) applies successfully to the stacking structure of 7 Å and 14 Å layers, whereas the alternative model of Banfield and Bailey (1996) is not applicable to the three samples (*e.g.* Figure 9). On the basis of Banfield and Bailey (1996), the type I*a* stacking in 7 Å layers is required to convert into the type I*b* stacking in adjacent 14 Å layers.

In the Soya sample, the stacking structure of 7 Å layers succeeded continuously to that of 14 Å layers by means of I*a* type stacking at both the left-hand and right-hand sides of lateral contact fronts (Figure 9b). Consequently, along with the severely disordered stacking as discussed above, the above observations imply

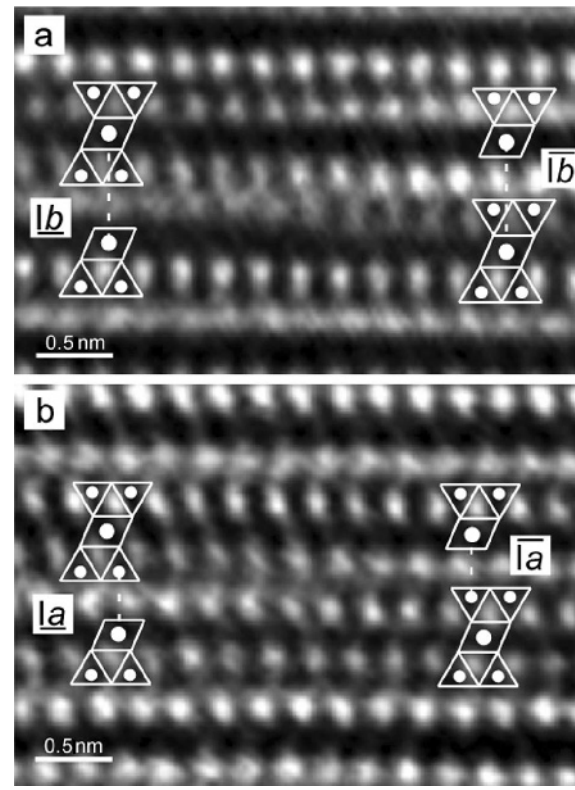

Figure 9. Magnified image of the lateral contact in (a) Ashio and (b) Soya. Schematic diagrams corresponding to the stacking structure are overlaid on HRTEM images.

https://doi.org/10.1346/CCMN.2016.0640205 Published online by Cambridge University Press

that the stacking relation between 7 Å and 14 Å layers as components in interstratification cannot be explained by the inheritance of polytypic groups during a solid-state transformation. The interstratified minerals of 7 Å and 14 Å layers observed in the present study are not part of an intermediate stage of topotactic transformation between the two minerals as described by Baronnet (1992), Xu and Veblen (1996), and Banfield and Bailey (1996).The present study assumed that the chemical compositions of each component layer are the same. The differences in chemical compositions of the component layers and the atomic-scale chemical heterogeneities may have to be taken into consideration. Further characterizations of individual component layers from the viewpoint of the chemical heterogeneity will be beneficial in clarifying the genesis of the samples.

Geological implications

The petrographic microscopic and TEM observations suggest that each chlorite sample studied here precipitated in veins directly from solutions, and were not affected by later modifications (*e.g*. Inoue *et al*., 2010; 2012), *i.e.* each sample was neoformed as opposed to the topotactic transformation from the precursor minerals. The formation temperatures were >190ºC, determined from homogenization temperatures of fluid inclusions in associated quartz and chlorite geothermometry (Table 1). Because of the relatively high-temperature precipitation of chlorites, the following is recognized: the component layers in chlorites with low Fe content (*e.g*. Ishikirizawa and Unotori) are basically 14 Å. Each structure is polytype II*bb*, which is the most stable structure of chlorite (Bailey, 1988b). Interlayering with different component layers was observed locally in HRTEM images, though the frequency was below the detection limit of XRD. The interstratified component layer appeared to be dehydrated smectite of 10 Å, and the interstratified structure involved two layers that form a regularly interstratified structure with 24 Å fringes such as corrensite. This type of interstratification has been documented in the saponite-to-chlorite series in various geologic regimes (*e.g*. Hillier, 1993; Beaufort *et al*., 1997; Murakami *et al*., 1999; Kogure *et al*., 2013).

In contrast, the present study highlights that the proportion of 7 Å layers increases with increasing Fe content, and the number of 7 Å layers can be >80% near the Fe end member. The chemical composition of 7 Å layers approximates Fe-rich berthierine. Berthierine is common in sedimentary rocks and is probably a precursor of chamosite during burial diagenesis. Natural occurrences show that the transformation of berthierine to chamosite occurs over a wide temperature range from 70ºC to 200ºC during burial diagenesis (*e.g*. Velde, 1985; Jahren and Aagaard, 1989; Hornibrook and Longstaffe, 1996). Experiments at relatively low temperature conditions (*e.g*. Mosser-Ruck *et al*., 2010) demonstrated that berthierine is stable at low temperatures and converts to chamosite at higher temperatures at >200ºC. In addition, high-temperature and high-pressure experiments on the stability of Fe-rich chlorite, including Fe-amesite composition (*e.g*. Chernosky *et al*., 1988; Parra *et al*., 2005; Vidal *et al*., 2005, and references therein), also suggested that the 7 Å phase appeared as a metastable phase and converted to 14 Å chlorite following the Ostwald step rule. More recently, Blanc *et al*. (2014) indicated, from their calorimetric measurements of Fe-rich chlorite and berthierine, that berthierine might transform into chlorite at higher temperatures, but the transformation temperature is dependent on the chemical composition of the two minerals. Although the thermal stability of berthierine is not resolved, the Fe-rich berthierine studied here precipitated as a metastable phase from solutions, based on the intensive irregularity of layer stacking as observed using HRTEM. Nevertheless, the fact that Fe-rich berthierine formed at higher temperatures than those in sedimentary environments indicates the necessity to reconsider the thermal stability of Fe-rich berthierine.

CONCLUSIONS

The present HRTEM study characterized chlorites which precipitated at temperatures from 190ºC to 320ºC in quartz veins of hydrothermal ore deposits. Low magnification HRTEM images showed that most of the samples exhibited interstratification between 7 Å, 14 Å, and (in some samples) smectite layers. The proportion of 7 Å layers increased progressively with Fe content, but independent of the formation temperatures. The proportion of 7 Å layers in the samples with Fe/(Fe+Mg) > 0.9 exceeds 80%. From the chemical point of view, the 7 Å layer was close to Fe-rich berthierine. Although berthierine has been considered to be a low-temperature phase of chlorite, the present study suggested that Fe-rich berthierine can form at temperatures higher than those in sedimentary environments. The stacking structures in the Fe-rich samples were characterized by disorder of 7 Å and 14 Å layers, differences in the polarity of the tetrahedral sheets, and a mixture of different polytypic structures, as indicated by HRTEM observations along Y_i directions of the structure. The results of this study suggest that the irregularity in the structure of chlorite samples was controlled by neither the Fe/(Fe+Mg) ratio nor the formation temperature; instead, the irregularity was controlled by the kinetic factors in the process of mineral precipitation under disequilibrium conditions.

ACKNOWLEDGMENTS

The authors are grateful to Tetsuro Yoneda of Hokkaido University and Atsuyuki Inoue of Chiba University for kindly providing the chlorite samples used in the present study; in particular to A. Inoue for providing unpublished microthermometric data of fluid inclusions.

The authors thank Michael A. Velbel, Alain Baronnet, and two anonymous reviewers for their valuable and constructive comments which improved this paper. S.I. was supported by a Research Fellowship of the Japan Society for the Promotion of Science (JSPS).

REFERENCES

Bailey, S.W. and Brown, G. (1962) Chlorite polytypism: I. Regular and semirandom one-layer structures. *American Mineralogist*, **47**, 819–850.

Bailey, S.W. (1969) Polytypism of trioctahedral 1:1 layer silicates. *Clays and Clay Minerals*, **17**, 355–371.

Bailey, S.W. (1988a) Chlorites: Structures and crystal chemistry. Pp. 347–403 in: *Hydrous Phyllosilcates (Exclusive of Micas)* (S.W. Bailey, editor). Reviews in Mineralogy, **19**, Mineralogical Society of America, Chantilly, Virginia, USA.

Bailey, S.W. (1988b) Structures and compositions of other trioctahedral 1: 1 phyllosilicates. Pp. 169–188 in: *Hydrous Phyllosilcates (Exclusive of Micas)* (S.W. Bailey, editor). Reviews in Mineralogy, **19**, Mineralogical Society of America, Chantilly, Virginia, USA.

Banfield, J.F. and Bailey, S.W. (1996) Formation of regularly interstratified serpentine-chlorite minerals by tetrahedral inversion in long-period serpentine polytypes. *American Mineralogist*, **81**, 79–91.

Baronnet, A. (1992) Polytypism and stacking disorder. Pp. 231–288 in: *Minerals and Reactions at the Atomic Scale: Transmission Electron Microscopy* (P.R. Buseck, editor). Reviews in Mineralogy, **27**, Mineralogical Society of America, Chantilly, Virginia, USA.

Beaufort, D., Baronnet, A., Lanson, B., and Meunier, A. (1997) Corrensite: A single phase or a mixed-layer phyllosilicate in the saponite-to-chlorite conversion series? A case study of Sancerre-Couy deep drill hole (France). *American Mineralogist*, **82**, 109–124.

Billault, V., Beaufort, D., Baronnet, A., and Lacharpagne, J. C. (2003) A nanopetrographic and textural study of grain-coating chlorites in sandstone reservoirs. *Clay Minerals*, **38**, 315–328.

Blanc, P., Gailhanou, H., Rogez, J., Mikaelian, G., Kawaji, H., Warmont, F., Gaboreau, S., Grangeon, S., Grenèche, J. M., Vieillard, P., Fialips, C., Giffaut, E., Gaucher, E., and Claret, F. (2014) Thermodynamic properties of chlorite and berthierine derived from calorimetric measurements. *Physics and Chemistry of Minerals*, **41**, 603–615.

Bourdelle, F., Benzerara, K., Beyssac, O., Cosmidis, J., Neuville, D. R., Brown, G.E., and Paineau, E. (2013) Quantification of the ferric/ferrous iron ratio in silicates by scanning transmission X-ray microscopy at the Fe $L_{2,3}$ edges. *Contributions to Mineralogy and Petrology*, **166**, 423–434.

Brindley, G.W. (1982) Chemical-compositions of berthierines – a review. *Clays and Clay Minerals*, **30**, 153–155.

Buddington, A.F. (1935) High-temperature mineral associations at shallow to moderate depths. *Economic Geology and the Bulletin of the Society of Economic Geologists*, **30**, 205–222.

Cassagnabère, A. (1998) Characterization and interpretation of kaolinite-to-dickite transition in Froy and Rind hydrocarbons reservoirs (North Sea, Norway). PhD Thesis, University of Poitiers, France, 237 pp.

Chernosky, J.V., Berman, R.G., and Bryndzia, L.T. (1988) Stability, phase relations, and thermodynamic properties of chlorite and serpentine group minerals. Pp. 295–346 in: *Hydrous Phyllosilcates (Exclusive of Micas)* (S.W. Bailey, editor). Reviews in Mineralogy, **19**, Mineralogical Society of America, Chantilly, Virginia, USA.

Foster, M.D. (1962) Interpretation of the composition and a classification of the chlorites. *U. S. Geological Survey Professional Paper*, **414-A**, 1–33.

Gregory, M.R. and Johnston, K.A. (1987) A nontoxic substitute for hazardous heavy liquids – aqueous sodium polytungstate ($3Na_2WO_4{\cdot}9WO_3{\cdot}H_2O$) solution (Note). *New Zealand Journal of Geology and Geophysics*, **30**, 317–320.

Hillier, S. (1993) Origin, diagenesis, and mineralogy of chlorite minerals in Devonian lacustrine mudrocks, Orcadian Basin, Scotland. *Clays and Clay Minerals*, **41**, 240–259.

Hornibrook, E.R. and Longstaffe, F.J. (1996) Berthierine from the Lower Cretaceous Clearwater Formation, Alberta, Canada. *Clays and Clay Minerals*, **44**, 1–21.

Iijima, A. and Matsumoto, R. (1982) Berthierine and chamosite in coal measures of Japan. *Clays and Clay Minerals*, **30**, 264–274.

Imai, H., Lee, M.S., Iida, K., Fujiki, Y., and Takenouchi, S. (1975) Geologic structure and mineralization of the xenothermal vein-type deposits in Japan. *Economic Geology*, **70**, 647–676.

Inoue, A., Meunier, A., Patrier-Mas, P., Rigault, C., Beaufort, D., and Vieillard, P. (2009) Application of chemical geothermometry to low-temperature trioctahedral chlorites. *Clays and Clay Minerals*, **57**, 371–382.

Inoue, A., Kurokawa, K., and Hatta, T. (2010) Application of chlorite geothermometry to hydrothermal alteration in Toyoha geothermal system, southwestern Hokkaido, Japan. *Resource Geology*, **60**, 52–70.

Inoue, A., Kurokawa, K., and Nitta, M. (2012) Environment of mineral-fluid interactions in the Toyoha hydrothermal system, southwestern Hokkaido, Japan. *Clay Science*, **16**, 59–81.

Jahren, J. and Aagaard, P. (1989) Compositional variations in diagenetic chlorites and illites, and relationships with formation-water chemistry. *Clay Minerals*, **24**, 157–170.

Jiang, W.T., Peacor, D.R., and Slack, J.F. (1992) Microstructures, mixed layering, and polymorphism of chlorite and retrograde berthierine in the Kidd Creek massive sulfide deposit, Ontario. *Clays and Clay Minerals*, **40**, 501–514.

Kilaas, R. (1998) Optimal and near-optimal filters in high-resolution electron microscopy. *Journal of Microscopy*, **190**, 45–51.

Kogure, T. and Banfield, J. F. (1998) Direct identification of the six polytypes of chlorite characterized by semi-random stacking. *American Mineralogist*, **83**, 925–930.

Kogure, T., Hybler, J., and Durovic, S. (2001) A HRTEM study of cronstedtite: determination of polytypes and layer polarity in trioctahedral 1:1 phyllosilicates. *Clays and Clay Minerals*, **49**, 310–317.

Kogure, T., Drits, V.A., and Inoue, S. (2013) Structure of mixed-layer corrensite-chlorite revealed by high-resolution transmission electron microcopy (HRTEM). *American Mineralogist*, **98**, 1253–1260.

Marks, L.D. (1996) Wiener-filter enhancement of noisy HREM images. *Ultramicroscopy*, **62**, 43-52.

Meunier, A. (2005) *Clays*. Springer, Berlin, 472 pp.

Moore, D.M. and Reynolds, R.C. (1989) *X-ray Diffraction and the Identification and Analysis of Clay Minerals*. Oxford University Press, New York, 332 pp.

Mosser-Ruck, R., Cathelineau, M., Guillaume, D., Charpentier, D., Rousset, D., Barres, O., and Michau, N. (2010) Effects of temperature, pH, and iron/clay and liquid/clay ratios on experimental conversion of dioctahedral smectite to berthierine, chlorite, vermiculite, or saponite. *Clays and Clay Minerals*, **58**, 280–291.

Murakami, T., Sato, T., and Inoue, A. (1999) HRTEM evidence for the process and mechanism of saponite-to-chlorite

conversion through corrensite. *American Mineralogist*, **84**, 1080–1087.

Nakamura, T. (1970) Mineral zoning and characteristic minerals in the polymetallic veins of the Ashio copper mine. Pp. 231–246 in: *Volcanism and Ore Genesis* (T. Tatsumi, editor), University of Tokyo Press, Tokyo.

Parra, T., Vidal, O., and Theye, T. (2005) Experimental data on the Tschermak substitution in Fe-chlorite. *American Mineralogist*, **90**, 359–370.

Reynolds, R. (1988) Mixed layer chlorite minerals. Pp. 601–629 in: *Hydrous Phyllosilcates (Exclusive of Micas)* (S.W. Bailey, editor). Reviews in Mineralogy, **19**, Mineralogical Society of America, Chantilly, Virginia, USA.

Reynolds, R.C., Distefano, M.P., and Lahann, R.W. (1992) Randomly interstratified serpentine/chlorite: Its detection and quantification by powder X-ray diffraction methods. *Clays and Clay Minerals*, **40**, 262–267.

Shikazono, N. (2003) *Geochemical and Tectonic Evolution of Arc-Backarc Hydrothermal Systems: Implication for the Origin of Kuroko and Epithermal Vein-type Mineralizations and the Global Geochemical Cycle*. Elsevier, Amsterdam, 463 pp.

Shirozu, H. (1978) Chlorite minerals. Pp. 243–264 in: *Clays and Clay Minerals of Japan* (T. Sudo and S. Shimoda, editors). Developments in Sedimentology, **26**. Elsevier Applied Science.

Shirozu, H. and Bailey, S.W. (1965) Chlorite polytypism: III. Crystal structure of an orthohexagnal iron chlorite. *American Mineralogist*, **50**, 868–885.

Slack, J.F. and Coad, P.R. (1989) Multiple hydrothermal and metamorphic events in the Kidd Creek volcanogenic massive sulphide deposit, Timmins, Ontario: Evidence from tourmalines and chlorites. *Canadian Journal of Earth Sciences*, **26**, 694–715.

Slack, J.F., Jiang, W.T., Peacor, D.R., and Okita, P.M. (1992) Hydrothermal and metamorphic berthierine from the Kidd Creek volcanogenic massive sulfide deposit, Timmins, Ontario. *The Canadian Mineralogist*, **30**, 1127–1142.

Velde, B. (1985) *Clay Minerals: A Physico-Chemical Explanation of their Occurrence.* Elsevier, Amsterdam, 427 pp.

Vidal, O., Parra, T., and Vieillard, P. (2005) Thermodynamic properties of the Tschermak solid solution in Fe-chlorite: Application to natural examples and possible role of oxidation. *American Mineralogist*, **90**, 347–358.

Xu, H.F. and Veblen, D.R. (1996) Interstratification and other reaction microstructures in the chlorite-berthierine series. *Contributions to Mineralogy and Petrology*, **124**, 291–301.

(*Received 15 March 2015; revised 13 April 2016; Ms. 976; AE: M.A. Velbel*)